Computational Studies of New Materials II: From Ultrafast Processes and Nanostructures to Optoelectronics, Energy Storage and Nanomedicine (2011), Chapter 14, 379-404, invited article, Eds. Thomas F. George, Daniel A. Jelski, Renat R. Letfullin and Guoping Zhang (World Scientific, Singapore)

Chapter 14

Nanoscale Resolution in the Near and Far Field Intensity Profile of Optical Dipole Radiation

Xin Li* and Henk F. Arnoldus†

Mississippi State University

**xl121@msstate.edu*

†*hfa1@msstate.edu*

Jie Shu

Rice University

js35@rice.edu

When an electric dipole moment rotates, the flow pattern of the emitted energy exhibits a vortex structure in the near field. The field lines of energy flow swirl around an axis which is perpendicular to the plane of rotation of the dipole. This rotation leads to an apparent shift of the dipole when viewed from the far field. The shift is of the order of the spatial extend of the vortex, which is about a fraction of an optical wavelength. We also show that when an image of the radiation is formed on an observation plane in the far field, the rotation of the field lines in the near field leads to a shift of the dipole image.

14.1. Introduction

When light is emitted by a localized source, it appears as if the light travels along straight lines from the source to the observer, when viewed from the far field (many wavelengths from the source). These light rays are the flow lines of energy, and they are usually referred to as optical rays. The rays are the orthogonal trajectories of the wave fronts. In the geometrical optics limit of light propagation certain terms in Maxwell's equations can be neglected under the assumption that the wavelength of

the light is small compared to other relevant distances. It can then be shown [1] that in a homogeneous medium, like the vacuum, the rays are straight lines, running from the source to the far field, and they coincide with the field lines of energy flow. However, when the light is detected within a fraction of a wavelength from the source, or with nanoscale precision at a larger distance, the geometrical optics limit does not apply, and we have to consider the exact solution of Maxwell's equations at all distances. The flow lines of energy will in general be curves. Far away from the source, each curve will asymptotically approach a straight line, but, when measured with nanoscale resolution, these asymptotic lines will not coincide with the optical rays. The rays run radially out from the source, but an asymptote of a field line of energy flow could be displaced with respect to this direction.

When the dimension of a localized source of radiation is small compared to the wavelength of the emitted light, then the source is in first approximation an electric dipole, located at the center of the source, and when viewed from outside the source, the radiation is identical to the radiation emitted by a point dipole. Also, radiation emitted by atoms and molecules is usually electric dipole radiation, and since atoms and molecules are much smaller than the wavelength of the light they emit, we can consider them as point sources. Since electric dipole radiation is the most elementary type of radiation, we shall consider the nanoscale structure of this type of radiation. We shall consider the spatial distribution of the energy flow in the near field, and we shall show that the curving of the field lines in the near field has an effect on the observable intensity profile in the far field, provided that the measurement is carried out with sub-wavelength resolution.

14.2. Electric Dipole Radiation

When the current density of a localized source oscillates harmonically with angular frequency ω, for instance when the source is placed in a laser beam oscillating at the same frequency ω, then the induced electric dipole moment has the form

$$\mathbf{d}(t) = d_{\mathrm{o}}\,\mathrm{Re}\,(\boldsymbol{\varepsilon}\, e^{-i\omega t})\ , \tag{14.1}$$

with $d_o > 0$ and $\boldsymbol{\varepsilon}$ a unit vector, normalized as $\boldsymbol{\varepsilon} \cdot \boldsymbol{\varepsilon}^* = 1$. The radiated electric field will also have a harmonic time dependence, and can be written as

$$\mathbf{E}(\mathbf{r},t) = \mathrm{Re}[\mathbf{E}(\mathbf{r})e^{-i\omega t}] \ , \tag{14.2}$$

with $\mathbf{E}(\mathbf{r})$ the complex amplitude. A similar expression holds for the magnetic field $\mathbf{B}(\mathbf{r},t)$. When the dipole is located at the origin of coordinates, the complex amplitudes of the electric and magnetic fields are given by [2]

$$\mathbf{E}(\mathbf{r}) = \frac{d_o k_o^3}{4\pi\varepsilon_o}\left\{\boldsymbol{\varepsilon} - (\boldsymbol{\varepsilon}\cdot\hat{\mathbf{r}})\hat{\mathbf{r}} + [\boldsymbol{\varepsilon} - 3(\boldsymbol{\varepsilon}\cdot\hat{\mathbf{r}})\hat{\mathbf{r}}]\frac{i}{q}\left(1+\frac{i}{q}\right)\right\}\frac{e^{iq}}{q} \ , \tag{14.3}$$

$$\mathbf{B}(\mathbf{r}) = -\frac{d_o k_o^3}{4\pi\varepsilon_o}\boldsymbol{\varepsilon}\times\hat{\mathbf{r}}\left(1+\frac{i}{q}\right)\frac{e^{iq}}{q} \ , \tag{14.4}$$

where $k_o = \omega/c$ is the wave number in free space and $\hat{\mathbf{r}}$ is a unit vector which is directed from the location of the dipole to the field point, represented by $\mathbf{r}$. We have also introduced the dimensionless variable $q = k_o r$, which represents the distance between the field point and the dipole. In this way, a distance of 2π in terms of q corresponds to a distance of one optical wavelength in terms of r. The properties of the electric dipole moment enter the expressions for $\mathbf{E}(\mathbf{r})$ and $\mathbf{B}(\mathbf{r})$ only through the complex-valued unit vector $\boldsymbol{\varepsilon}$ (apart from an overall d_o).

14.3. Energy Flow and the Poynting Vector

In an electromagnetic field the energy flow is determined by the Poynting vector, defined as

$$\mathbf{S}(\mathbf{r},t) = \frac{1}{\mu_o}\mathbf{E}(\mathbf{r},t)\times\mathbf{B}(\mathbf{r},t) \ , \tag{14.5}$$

for propagation in vacuum. If dA is an infinitesimal surface element at the position $\mathbf{r}$, with unit normal $\hat{\mathbf{n}}$, then the power flowing through dA is

equal to $\mathrm{d}P = \mathbf{S}\cdot\hat{\mathbf{n}}\mathrm{d}A$. Therefore, at position $\mathbf{r}$ the energy flows into the direction of the Poynting vector $\mathbf{S}$. For time-harmonic fields, as in Eq. (14.2), the Poynting vector simplifies to

$$\mathbf{S}(\mathbf{r}) = \frac{1}{2\mu_{\mathrm{o}}}\mathrm{Re}\,[\mathbf{E}(\mathbf{r})\times\mathbf{B}(\mathbf{r})^*]\ , \tag{14.6}$$

and here terms that oscillate at twice the optical frequency ω have been dropped, since these average to zero in an experiment, on a time scale of an optical cycle. The Poynting vector in Eq. (14.6) only involves the complex amplitudes, rather than the fields themselves, and $\mathbf{S}(\mathbf{r})$ is independent of time t.

With expressions (14.3) and (14.4) the Poynting vector for the radiation emitted by a dipole can be evaluated immediately. We obtain

$$\mathbf{S}(\mathbf{r}) = \frac{3P_{\mathrm{o}}}{8\pi r^2}\left\{\zeta(\theta,\phi)\hat{\mathbf{r}} - \frac{2}{q}\left(1+\frac{1}{q^2}\right)\mathrm{Im}\,[(\hat{\mathbf{r}}\cdot\boldsymbol{\varepsilon})\boldsymbol{\varepsilon}^*]\right\}\ , \tag{14.7}$$

where θ and ϕ are the angles of the observation point $\mathbf{r}$ in a spherical coordinate system. The function $\zeta(\theta,\phi)$ is given by

$$\zeta(\theta,\phi) = 1-(\hat{\mathbf{r}}\cdot\boldsymbol{\varepsilon})(\hat{\mathbf{r}}\cdot\boldsymbol{\varepsilon}^*)\ , \tag{14.8}$$

and

$$P_{\mathrm{o}} = \frac{ck_{\mathrm{o}}^4}{12\pi\varepsilon_{\mathrm{o}}}d_{\mathrm{o}}^2\ , \tag{14.9}$$

is the power emitted by the dipole. The unit vector $\hat{\mathbf{r}}$ is in spherical coordinates

$$\hat{\mathbf{r}} = (\mathbf{e}_x\cos\phi + \mathbf{e}_y\sin\phi)\sin\theta + \mathbf{e}_z\cos\theta\ , \tag{14.10}$$

and this determines the dependence of $\zeta(\theta,\phi)$ on θ and ϕ, given the dipole moment vector $\boldsymbol{\varepsilon}$.

When we take $\mathrm{d}A$ as part of a sphere, centered around the origin, and with radius r, then $\mathrm{d}A = r^2\mathrm{d}\Omega$, and the radiated power per unit solid angle becomes

$$\frac{\mathrm{d}P}{\mathrm{d}\Omega} = r^2 \mathbf{S}(\mathbf{r}) \cdot \hat{\mathbf{r}} \ . \tag{14.11}$$

With Eq. (14.7) this becomes

$$\frac{\mathrm{d}P}{\mathrm{d}\Omega} = \frac{3P_\mathrm{o}}{8\pi} \zeta(\theta, \phi) \ , \tag{14.12}$$

since $(\hat{\mathbf{r}} \cdot \boldsymbol{\varepsilon}) \boldsymbol{\varepsilon}^* \cdot \hat{\mathbf{r}}$ is real. The emitted power per unit solid angle is independent of *r*, and this may give the impression that the power flows radially outward, as in the geometrical optics limit of light propagation. We shall see below that this is usually not the case.

When vector $\boldsymbol{\varepsilon}$ in Eq. (14.1) is real, the dipole moment is $\mathbf{d}(t) = d_\mathrm{o} \boldsymbol{\varepsilon} \cos(\omega t)$. This corresponds to a linear dipole moment, oscillating back and forth along an axis through vector $\boldsymbol{\varepsilon}$. For this case, the Poynting vector becomes

$$\mathbf{S}(\mathbf{r}) = \frac{3P_\mathrm{o}}{8\pi r^2} \zeta(\theta, \phi) \hat{\mathbf{r}} \ , \tag{14.13}$$

since $(\hat{\mathbf{r}} \cdot \boldsymbol{\varepsilon}) \boldsymbol{\varepsilon}^*$ is real. Then $\mathbf{S}(\mathbf{r})$ is proportional to $\hat{\mathbf{r}}$ at any field point, and hence the power flow is exactly in the radial direction. The field lines of $\mathbf{S}(\mathbf{r})$, which are the field lines of energy flow, are straight lines, running from the location of the dipole to infinity.

14.4. Elliptical Dipole Moment

In its most general state of oscillation, the dipole moment $\mathbf{d}(t)$ traces out an ellipse in a plane [3,4]. We take this plane to be the *xy*-plane, and we parametrize vector $\boldsymbol{\varepsilon}$ as

$$\boldsymbol{\varepsilon} = -\frac{1}{\sqrt{\beta^2 + 1}} (\beta \mathbf{e}_x + i \mathbf{e}_y) \ , \tag{14.14}$$

with β real. The parametrization is chosen such that for $\beta = \pm 1$, vector $\boldsymbol{\varepsilon}$ reduces to the standard spherical unit vectors

$$\mathbf{e}_{\pm 1} = -\frac{1}{\sqrt{2}}(\pm \mathbf{e}_x + i\mathbf{e}_y) \ , \tag{14.15}$$

with respect to the z-axis. With $\boldsymbol{\varepsilon}$ from Eq. (14.14), the dipole moment becomes

$$\mathbf{d}(t) = -\frac{d_{\mathrm{o}}}{\sqrt{\beta^2+1}}[\beta \mathbf{e}_x \cos(\omega t) + \mathbf{e}_y \sin(\omega t)] \ . \tag{14.16}$$

As time progresses, vector $\mathbf{d}(t)$ follows the contour of an ellipse, as shown in Fig. 14.1. For $\beta = \pm 1$ the ellipse reduces to a circle. When β is positive, the rotation is counterclockwise as in the figure, which is the positive direction with the z-axis, as given by the right-hand rule. For $\beta < 0$ the rotation is in the opposite direction. For $\beta = 0$, vector $\boldsymbol{\varepsilon}$ becomes $-i\mathbf{e}_y$, and the oscillation is linear along the y-axis. In the limit $\beta \to \pm\infty$ we have $\boldsymbol{\varepsilon} \to \mp \mathbf{e}_x$, and the oscillation is linear along the x-axis.

For an elliptical dipole in the xy-plane, the function $\zeta(\theta,\phi)$ from Eq. (14.8) becomes

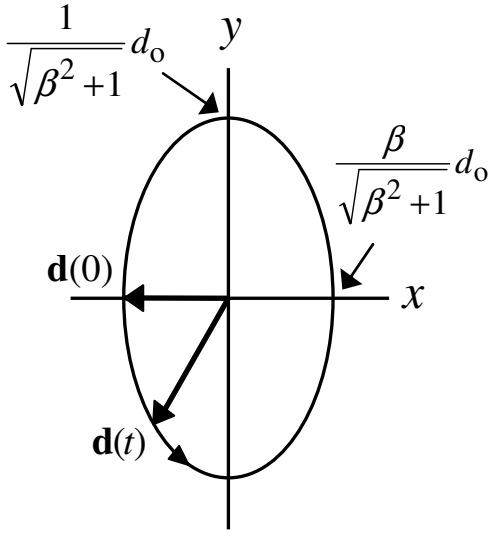

Fig. 14.1. In its most general state of oscillation, the dipole moment $\mathbf{d}(t)$ rotates along an ellipse. The parameter β (positive in the figure) determines the lengths of the major and minor axes, as shown in the figure, and the sign of β determines the direction of rotation.

$$\zeta(\theta,\phi) = 1 - \frac{1}{2}\sin^2\theta\left[1 + \frac{\beta^2 - 1}{\beta^2 + 1}\cos(2\phi)\right] . \qquad (14.17)$$

This function is, apart from an overall constant, the emitted power per unit solid angle into the direction (θ,ϕ), according to Eq. (14.12). For the Poynting vector, Eq. (14.7), we find

$$\mathbf{S}(\mathbf{r}) = \frac{3P_0}{8\pi r^2}\left\{\zeta(\theta,\phi)\hat{\mathbf{r}} + \frac{2}{q}\left(1 + \frac{1}{q^2}\right)\frac{\beta}{\beta^2 + 1}\mathbf{e}_\phi \sin\theta\right\} , \quad (14.18)$$

with

$$\mathbf{e}_\phi = -\mathbf{e}_x \sin\phi + \mathbf{e}_y \cos\phi . \qquad (14.19)$$

The term proportional to $\hat{\mathbf{r}}$ is responsible for the radial power outflow, and the term with $\mathbf{e}_\phi$ gives a rotation in the flow of energy around the z-axis. Close to the dipole this term is of order r^{-5}, whereas the radial term is of order r^{-2}. Therefore, in the near field the rotation will dominate the energy flow pattern, even though this rotation does not contribute to the power outflow at any distance from the dipole. In the limit of a linear dipole, $\beta = 0$ or $\beta \to \infty$, the term with $\mathbf{e}_\phi$ vanishes, and the Poynting vector only has a radial component, corresponding to power flowing radially outward from the dipole, without any swirling around the z-axis.

14.5. Field Lines of the Poynting Vector

In order to investigate in detail the energy flow out of a dipole, we consider the field lines of the Poynting vector $\mathbf{S}(\mathbf{r})$. Expression (14.18) for $\mathbf{S}(\mathbf{r})$ determines a vector field in space, and a field line of $\mathbf{S}(\mathbf{r})$ is a curve for which at any point along the curve the vector $\mathbf{S}(\mathbf{r})$ is on its tangent line. When $\mathbf{r}$ is a point on the field line, then we can parametrize such a field line as $\mathbf{r}(u)$, with u a dummy variable. A field line is determined only by the direction of $\mathbf{S}(\mathbf{r})$, and not its magnitude, and hence a field line is a solution of

$$\frac{\mathrm{d}\mathbf{r}}{\mathrm{d}u} = f(\mathbf{r})\mathbf{S}(\mathbf{r}) , \qquad (14.20)$$

with $f(\mathbf{r})$ any positive function of $\mathbf{r}$. Equation (14.19) is an autonomous differential equation, since the variable u does not appear on the right-hand side. The variable u itself has no physical significance.

We now use spherical coordinates (q,θ,ϕ) to represent a point $\mathbf{r}$, so that $\mathbf{r}=(q/k_{\mathrm{o}})\hat{\mathbf{r}}$, with $\hat{\mathbf{r}}$ given by Eq. (14.10). For a point on a field line, q, θ and ϕ then become functions of u, and when we write out Eq. (14.20) we obtain

$$\frac{\mathrm{d}q}{\mathrm{d}u}=k_{\mathrm{o}}f(\mathbf{r})\hat{\mathbf{r}}\cdot\mathbf{S}(\mathbf{r})\ , \tag{14.21}$$

$$q\frac{\mathrm{d}\theta}{\mathrm{d}u}=k_{\mathrm{o}}f(\mathbf{r})\mathbf{e}_{\theta}\cdot\mathbf{S}(\mathbf{r})\ , \tag{14.22}$$

$$q\sin\theta\frac{\mathrm{d}\phi}{\mathrm{d}u}=k_{\mathrm{o}}f(\mathbf{r})\mathbf{e}_{\phi}\cdot\mathbf{S}(\mathbf{r})\ , \tag{14.23}$$

with

$$\mathbf{e}_{\theta}=(\mathbf{e}_x\cos\phi+\mathbf{e}_y\sin\phi)\cos\theta-\mathbf{e}_z\sin\theta\ . \tag{14.24}$$

For the function $f(\mathbf{r})$ we take $8\pi r^2/(3P_{\mathrm{o}}k_{\mathrm{o}})$, and with Eq. (14.18) we then find the set of equations

$$\frac{\mathrm{d}q}{\mathrm{d}u}=\zeta(\theta,\phi)\ , \tag{14.25}$$

$$\frac{\mathrm{d}\theta}{\mathrm{d}u}=0\ , \tag{14.26}$$

$$\frac{\mathrm{d}\phi}{\mathrm{d}u}=\frac{2}{q^2}\left(1+\frac{1}{q^2}\right)\frac{\beta}{\beta^2+1}\ , \tag{14.27}$$

for the coordinates q, θ and ϕ as functions of u for points on a field line.

From Eq. (14.26) it follows that θ is constant along a field line, and let us indicate this constant by θ_{o}. Any field line starts at the location of the dipole, and we then see that it remains on a cone which has an angle

θ_o with the z-axis. Then we can replace θ by θ_o on the right-hand side of Eq. (14.25), and divide Eq. (14.27) by Eq. (14.25). This yields

$$\frac{d\phi}{dq} = \frac{2}{q^2}\left(1+\frac{1}{q^2}\right)\frac{1}{\zeta(\theta_o,\phi)}\frac{\beta}{\beta^2+1} \ . \tag{14.28}$$

When we see ϕ as a function of q, rather than u, this is a nonlinear first-order equation for the function $\phi(q)$. The equation is separable, and is most easily solved by considering q as a function of ϕ. The result is [5]

$$q(\phi) = \frac{1}{[(1+\frac{1}{4}A^2)^{\frac{1}{2}}+\frac{1}{2}A]^{\frac{1}{3}} - [(1+\frac{1}{4}A^2)^{\frac{1}{2}}-\frac{1}{2}A]^{\frac{1}{3}}} \ , \tag{14.29}$$

where A is a function of ϕ, defined as

$$A = \frac{3}{8}\left(\beta-\frac{1}{\beta}\right)\sin^2\theta_o\,[\sin(2\phi)-\sin(2\phi_o)]$$
$$-\frac{3}{2}\left(\beta+\frac{1}{\beta}\right)\left(1-\frac{1}{2}\sin^2\theta_o\right)(\phi-\phi_o) \ . \tag{14.30}$$

We see from Eq. (14.28) that for q large we have $d\phi/dq \to 0$, and therefore ϕ approaches a constant ϕ_o at a large distance. This is angle ϕ_o in the expression for A, and this ϕ_o serves as the integration constant. Angle ϕ is now the free parameter, and it follows from the derivation in Ref. [5] that, given ϕ_o, angle ϕ has to be taken in the range

$$-\infty < \phi < \phi_o \quad , \quad \beta > 0 \ , \tag{14.31}$$

$$\phi_o < \phi < \infty \quad , \quad \beta < 0 \ . \tag{14.32}$$

Therefore, each field line is determined by a choice of θ_o and ϕ_o, which are the values of θ and ϕ at a large distance.

We indicate by $\bar{x} = k_o x$, $\bar{y} = k_o y$ and $\bar{z} = k_o z$ the dimensionless Cartesian coordinates of a field point. We then have along a field line

$$\bar{x}(\phi) = q(\phi)\sin\theta_{\rm o}\cos\phi \ , \tag{14.33}$$

$$\bar{y}(\phi) = q(\phi)\sin\theta_{\rm o}\sin\phi \ , \tag{14.34}$$

$$\bar{z}(\phi) = q(\phi)\cos\theta_{\rm o} \ , \tag{14.35}$$

with ϕ the free variable, and $q(\phi)$ given by Eq. (14.29). Figure 14.2 shows several field lines for $\theta_{\rm o} = \pi/4$ and $\theta_{\rm o} = 3\pi/4$ and for different values of $\phi_{\rm o}$. For the figure we took $\beta = 1$, which corresponds to a circular dipole moment, rotating counterclockwise in the *xy*-plane. The field lines swirl around the *z*-axis with the same orientation as the rotation of the dipole moment. The field line pattern has a vortex structure, with the dipole at the center of the vortex. All field lines wind around the *z*-axis, while remaining on a cone. The scale in the figure is such that 2π corresponds to one optical wavelength, and we see that the spatial extend of the vortex is well below a wavelength. Figure 14.3 shows field lines for $\beta = 1$, so for the same dipole as in Fig. 14.2, but now for different values of $\theta_{\rm o}$. Angle $\phi_{\rm o}$ is the same for all field lines, and is taken as $\pi/2$. Therefore, all field lines approach asymptotically a straight line parallel to the positive *y*-axis.

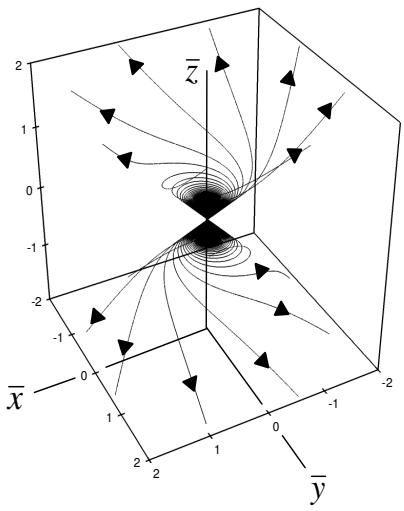

Fig. 14.2. The figure shows several field lines of the Poynting vector for a circular dipole, with a dipole moment that rotates counterclockwise in the *xy*-plane. Each field line lies on a cone which makes an angle of 45º with the *z*-axis.

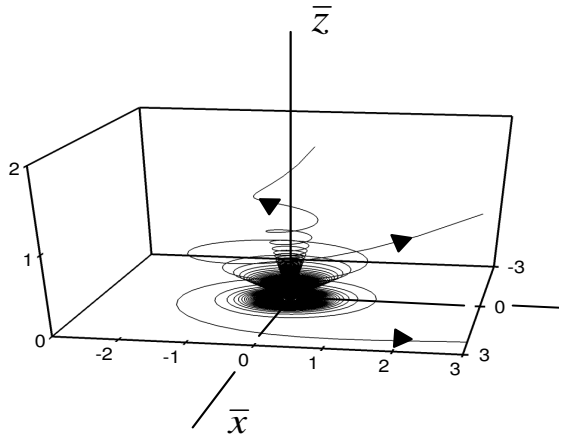

Fig. 14.3. The figure shows field lines for the same dipole as in Fig. 14.2, but now for different values of θ_o, and with $\phi_o = \pi/2$ for all field lines.

The result for the field lines depends parametrically on the value of β. For $\beta = 1$ the field lines show a vortex structure near the location of the dipole, as illustrated in Figs. 14.2 and 14.3, and the dimension of this vortex is a fraction of a wavelength. For $\beta \to 0$ and $\beta \to \infty$ the ellipse reduces to a line, and the oscillation of the dipole moment becomes linear. As shown above, for a linear dipole the field lines are straight lines emanating from the dipole. In order to see the transition from the vortex pattern for a circular dipole to the straight-line pattern for a linear dipole we have graphed field lines for three values of β in Fig. 14.4. It is seen from the figure that when β decreases from unity to zero, the size of the vortex diminishes, until it reaches a point for $\beta = 0$. For $\beta = 1$, the field lines bend around the *z*-axis over an extend of about a wavelength from the dipole. For smaller values of β, the field line becomes straight already in the very neighborhood of the dipole.

14.6. Field Lines in the Far Field

At a distance of many wavelengths from the dipole, each field line approaches a straight line, as can be seen from the figures above. This line, however, does not appear to come exactly from the location of the dipole, but it is slightly displaced with respect to the radial direction, as

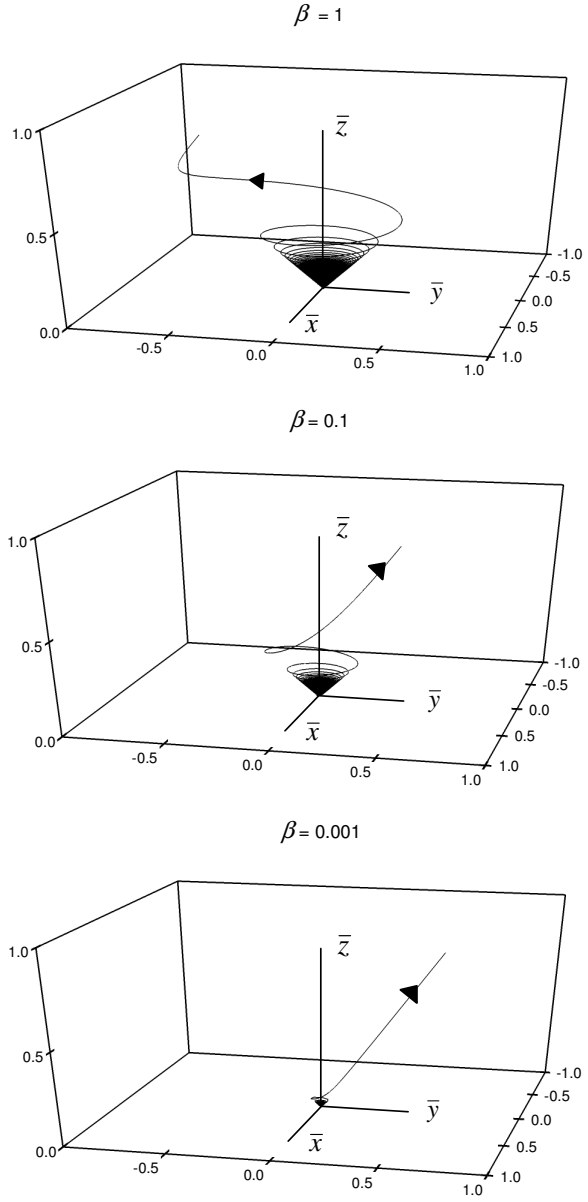

Fig. 14.4. Shown are field lines for dipoles with different values of β. For each, $\theta_o = \pi/4$ and $\phi_o = \pi/2$.

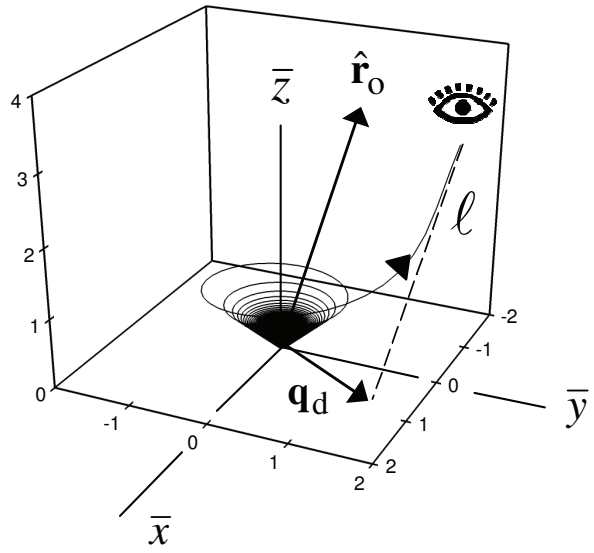

Fig. 14.5. Due to the rotation of a field line near the source, it appears as if the source is displaced when viewed from the far field.

illustrated in Fig. 14.5. For an observer, indicated by the eye in the figure, the field line of energy flow seems to come from a point in the *xy*-plane that does not coincide with the position of the source, and hence it appears as if the source is displaced with respect to its actual position. This apparent displacement, indicated by the displacement vector $\mathbf{q}_d$, is a result of the rotation of the field lines near the source, and as such this near field effect should be observable in the far field.

In order to compute this displacement, we consider q as the independent variable along a field line, rather than ϕ, even though in the explicit solution (14.29) it is the other way around. For q large, ϕ approaches the value ϕ_o, and the value of θ along a field line is θ_o at any point. Therefore, for q large we can expand ϕ in an asymptotic series as $\phi(q) = \phi_o + c_1/q + c_2/q^2 \ldots$, with the coefficients c_1, c_2, ... to be determined. In expression (17) for $\zeta(\theta,\phi)$ we set $\theta = \theta_o$ and for ϕ we substitute the asymptotic expansion. This gives $\zeta(\theta_o,\phi) = \zeta(\theta_o,\phi_o)$ + $\ddots$ $(1/q)$. We use this to expand the right-hand side of Eq. (14.28), which yields

$$\frac{\mathrm{d}\phi}{\mathrm{d}q} = \frac{1}{q^2}\,\frac{1}{\zeta(\theta_\mathrm{o},\phi_\mathrm{o})}\,\frac{2\beta}{\beta^2+1} + \ddots\left(\frac{1}{q^3}\right). \tag{14.36}$$

The right-hand side of Eq. (14.36) is an asymptotic series in q, and term-by-term integration gives

$$\phi(q) = \phi_\mathrm{o} - \frac{1}{q}\,Y(\theta_\mathrm{o},\phi_\mathrm{o};\beta) + \ldots\,, \tag{14.37}$$

where we have set

$$Y(\theta_\mathrm{o},\phi_\mathrm{o};\beta) = \frac{1}{\zeta(\theta_\mathrm{o},\phi_\mathrm{o})}\,\frac{2\beta}{\beta^2+1}\,, \tag{14.38}$$

which is a constant along a field line.

Equations (14.33)–(14.35) give the Cartesian coordinates of a point on a field line. We now view q as the independent variable, and we expand $\cos\phi$ and $\sin\phi$ in Eqs. (14.33) and (14.34) with the help of Eq. (14.37). We then obtain

$$\cos\phi(q) = \cos\phi_\mathrm{o} + \frac{1}{q}\,Y(\theta_\mathrm{o},\phi_\mathrm{o};\beta)\sin\phi_\mathrm{o} + \ldots\,, \tag{14.39}$$

$$\sin\phi(q) = \sin\phi_\mathrm{o} - \frac{1}{q}\,Y(\theta_\mathrm{o},\phi_\mathrm{o};\beta)\cos\phi_\mathrm{o} + \ldots\,. \tag{14.40}$$

For a point on a field line, q is the dimensionless distance between this point and the origin of coordinates. When the terms represented by ellipses in Eq. (14.37) are omitted, parameter q loses this significance. Therefore, we shall write t instead of q. Equations (14.33)–(14.35) then become

$$\bar{x} = \sin\theta_\mathrm{o}[t\cos\phi_\mathrm{o} + Y(\theta_\mathrm{o},\phi_\mathrm{o};\beta)\sin\phi_\mathrm{o}]\,, \tag{14.41}$$

$$\bar{y} = \sin\theta_\mathrm{o}[t\sin\phi_\mathrm{o} - Y(\theta_\mathrm{o},\phi_\mathrm{o};\beta)\cos\phi_\mathrm{o}]\,, \tag{14.42}$$

$$\bar{z} = t\cos\theta_{\mathrm{o}} \ . \tag{14.43}$$

For a given observation direction $(\theta_{\mathrm{o}},\phi_{\mathrm{o}})$, these Cartesian coordinates are linear functions of t, and hence Eqs. (14.41)–(14.43) are the parameter equations of a straight line. This is line ℓ in Fig. 14.5, which is the asymptote of the field line in the direction $(\theta_{\mathrm{o}},\phi_{\mathrm{o}})$. Vector $\hat{\mathbf{r}}_{\mathrm{o}}$ in Fig. 14.5 is the unit vector in the $(\theta_{\mathrm{o}},\phi_{\mathrm{o}})$ direction, which follows from Eq. (14.10) by replacing (θ,ϕ) by $(\theta_{\mathrm{o}},\phi_{\mathrm{o}})$. When we introduce the vector

$$\mathbf{q}_{\mathrm{d}} = Y(\theta_{\mathrm{o}},\phi_{\mathrm{o}};\beta)\sin\theta_{\mathrm{o}}(\mathbf{e}_x\sin\phi_{\mathrm{o}} - \mathbf{e}_y\cos\phi_{\mathrm{o}}) \ , \tag{14.44}$$

then Eqs. (14.41)–(14.43) can be written in vector form as

$$\mathbf{q} = \mathbf{q}_{\mathrm{d}} + t\hat{\mathbf{r}}_{\mathrm{o}} \ , \tag{14.45}$$

where $\mathbf{q} = k_{\mathrm{o}}\mathbf{r}$ is a point on the line ℓ. According to Eq. (14.43), $t = 0$ gives $\bar{z} = 0$, so this corresponds to the intersection point of ℓ and the xy-plane. The position vector of this point is $\mathbf{q}_{\mathrm{d}}$, as follows from Eq. (14.45), and therefore vector $\mathbf{q}_{\mathrm{d}}$ is the displacement vector of the source as shown in Fig. 14.5. It represents the apparent position of the source in the xy-plane, when viewed from the far field. From Eqs. (14.10) and (14.44) we see that $\mathbf{q}_{\mathrm{d}}\cdot\hat{\mathbf{r}}_{\mathrm{o}} = 0$, so $\mathbf{q}_{\mathrm{d}}$ is perpendicular to $\hat{\mathbf{r}}_{\mathrm{o}}$.

14.7. The Displacement

The magnitude of the displacement vector $\mathbf{q}_{\mathrm{d}}$ is given by

$$q_{\mathrm{d}} = \frac{2|\beta|}{\beta^2+1}\frac{\sin\theta_{\mathrm{o}}}{\zeta(\theta_{\mathrm{o}},\phi_{\mathrm{o}})} \ , \tag{14.46}$$

with $\zeta(\theta_{\mathrm{o}},\phi_{\mathrm{o}})$ given by Eq. (14.17). This source displacement depends on the observation angles θ_{o} and ϕ_{o}, and on the parameter β of the ellipse. For observation along the z-axis we have $\sin\theta_{\mathrm{o}} = 0$ and the

displacement is zero. As a function of θ_o, the displacement is maximum for $\theta_o = \pi/2$, so for observation along the *xy*-plane. In the *xy*-plane and for a given β, the displacement depends on the location in the *xy*-plane, e.g., on the angle ϕ_o. We find that the displacement is maximum for $\cos(2\phi_o) = 1$ when $|\beta| > 1$, and for $\cos(2\phi_o) = -1$ when $|\beta| < 1$. From Fig. 14.1 we then see that this corresponds to an observation along the major axis of the ellipse in both cases. In this direction, the displacement is given by

$$q_d = \begin{cases} 2|\beta| & , \quad |\beta| > 1 \\ \dfrac{2}{|\beta|} & , \quad |\beta| < 1 \end{cases} , \tag{14.47}$$

for a given β. For a circular dipole we have $|\beta| = 1$, and the maximum displacement is $q_d = 2$. For $\beta \to 0$ or $\beta \to \infty$ the eccentricity of the ellipse increases and the dipole becomes more linear. We then have $q_d > 2$ and the displacement can grow without bounds when the dipole approaches a linear dipole.

14.8. Intensity in the Image Plane

The observation direction (θ_o, ϕ_o) can be represented by a unit vector $\hat{\mathbf{r}}_o$, as in Fig. 14.5. We now consider an observation plane, shown in Fig. 14.6, which is a plane perpendicular to $\hat{\mathbf{r}}_o$, and a distance r_o away from the dipole. The origin of coordinates in this plane is represented by the vector $\mathbf{r}_o$. We then define λ and μ axes in this plane, such that the axes run into the direction of the the spherical unit vectors $\mathbf{e}_{\theta_o}$ and $\mathbf{e}_{\phi_o}$, as shown in the figure. Therefore, λ and μ are the Cartesian coordinates of a point in this plane, and the position vector $\mathbf{r}$ of a point in this plane can be written as

$$\mathbf{r} = \mathbf{r}_o + \lambda \mathbf{e}_{\theta_o} + \mu \mathbf{e}_{\phi_o} . \tag{14.48}$$

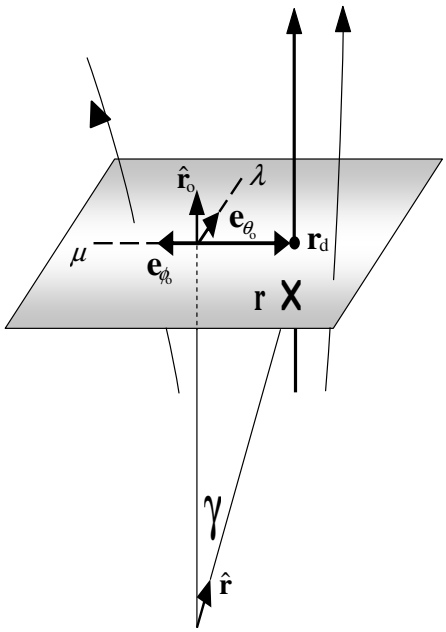

Fig. 14.6. The figure shows the coordinate system for the image plane and several field lines of the Poynting vector. Point **r** in the plane, represented by ✕, has Cartesian coordinates (λ, μ).

The dimensionless displacement vector (14.44) is a vector in this plane, and can be expressed as

$$\mathbf{q}_{\mathrm{d}} = -\mathbf{e}_{\phi_{\mathrm{o}}} Y(\theta_{\mathrm{o}}, \phi_{\mathrm{o}}; \beta) \sin\theta_{\mathrm{o}} \ . \tag{14.49}$$

The corresponding vector $\mathbf{r}_{\mathrm{d}} = \mathbf{q}_{\mathrm{d}} / k_o$ is shown in the figure. Therefore, the displacement vector is along the μ-axis. The asymptote ℓ of the field line for this direction $(\theta_{\mathrm{o}}, \phi_{\mathrm{o}})$ goes through the point $\mathbf{r}_{\mathrm{d}}$, and when the distance r_{o} is sufficiently large, the field line through this point is perpendicular to the observation plane.

When an image is formed on the observation plane, or image plane, it may be expected that the major contribution comes from the field lines in the neighborhood of $\mathbf{r}_{\mathrm{d}}$, since these cross the plane almost perpendicularly. In that case, the image in this plane would be

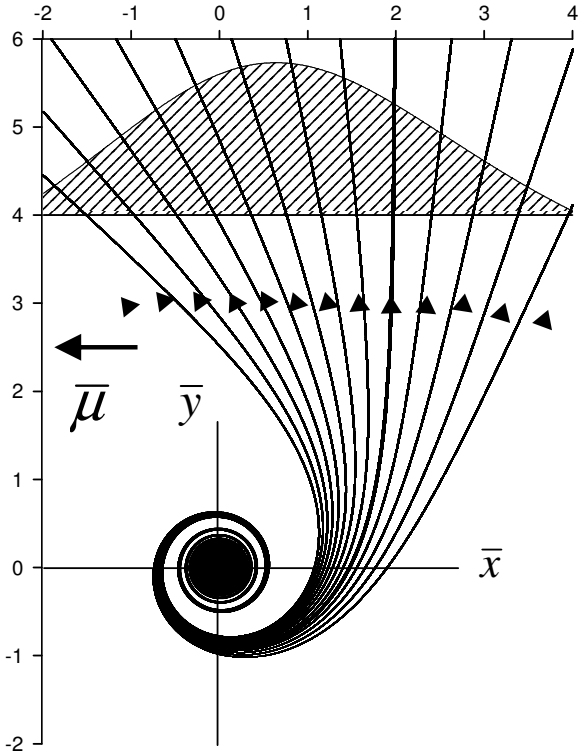

Fig. 14.7. Field lines of the Poynting vector in the *xy*-plane for a dipole moment which rotates in the *xy*-plane are shown. They swirl around the origin numerous times, and are then incident upon the image plane. The intensity distribution on the image plane shows a maximum in the neighborhood of the central field line for this direction, which goes through the point $\overline{x} = 2$ on the image plane.

shifted over $\mathbf{r}_{\mathrm{d}}$ with respect to the origin, and this shift would then be the same as the virtual displacement of the dipole in the *xy*-plane. However, since a bundle of field lines passing through this plane determines the image, rather than the single field line from Fig. 14.5, the image of the dipole is not necessarily exactly located at the position $\mathbf{r}_{\mathrm{d}}$. Figure 14.7 shows a bundle of field lines and the corresponding intensity distribution over a plane (defined below), and we observe that indeed the maximum of the image does not coincide with the displacement of the corresponding field line for this case ($\mathbf{q}_{\mathrm{d}} = 2\mathbf{e}_x$). It should also be noted that the shift in the *xy*-plane is defined through the extrapolation of the

asymptote ℓ of the field line in the observation direction, as in Fig. 14.5, and, from an experimental point of view, this may not be a directly observable shift.

In order to investigate this issue in detail, we now consider the intensity distribution over the image plane. Since $\hat{\mathbf{r}}_\mathrm{o}$ is the unit normal vector at all points in the image plane, the intensity (power per unit area) at point **r** is

$$I(\mathbf{r}_\mathrm{o};\lambda,\mu) = \mathbf{S}(\mathbf{r})\cdot\hat{\mathbf{r}}_\mathrm{o} \ . \tag{14.50}$$

This intensity depends on r_o, the distance between the source and the image plane, the observation direction $(\theta_\mathrm{o},\phi_\mathrm{o})$, and the coordinates λ and μ of point **r** in the plane. In addition, it depends parametrically on the parameter β of the ellipse.

We introduce dimensionless coordinates $\overline{\lambda} = k_\mathrm{o}\lambda$ and $\overline{\mu} = k_\mathrm{o}\mu$ in the observation plane, and the dimensionless distance between the origin of the plane and the dipole is $q_\mathrm{o} = k_\mathrm{o} r_\mathrm{o}$. For point **r** in the plane we then have $q = k_\mathrm{o} r$, and the relation to its Cartesian $(\overline{\lambda},\overline{\mu})$ is

$$q = \sqrt{q_\mathrm{o}^2 + \overline{\lambda}^2 + \overline{\mu}^2} \ . \tag{14.51}$$

Putting everything together yields [6]

$$I(\mathbf{r}_\mathrm{o};\lambda,\mu) = I_\mathrm{o}\left(\frac{q_\mathrm{o}}{q}\right)^3 \left\{1 - \frac{1}{q^2}\frac{1}{1+\beta^2}\right.$$

$$\times\left[\beta^2(\overline{\rho}\cos\phi_\mathrm{o} - \overline{\mu}\sin\phi_\mathrm{o})^2 + (\overline{\rho}\sin\phi_\mathrm{o} + \overline{\mu}\cos\phi_\mathrm{o})^2\right]$$

$$\left. - \frac{1}{q_\mathrm{o} q}\left(1+\frac{1}{q^2}\right)\frac{2\beta}{\beta^2+1}\overline{\mu}\sin\theta_\mathrm{o}\right\} \ , \tag{14.52}$$

for the intensity distribution in an observation plane for the case of an elliptical dipole moment, rotating in the *xy*-plane. In Eq. (14.52) we use the abbreviation

$$\overline{\rho} = q_{\rm o} \sin\theta_{\rm o} + \overline{\lambda} \cos\theta_{\rm o} \ , \tag{14.53}$$

and the overall factor $I_{\rm o}$ is given by

$$I_{\rm o} = \frac{3P_{\rm o}}{8\pi r_{\rm o}^2} \ . \tag{14.54}$$

The first two lines in Eq. (14.52) come from the angular dependence of the emitted power, which is accounted for by the function $\zeta(\theta,\phi)$ in Eq. (14.12) for $\mathrm{d}P/\mathrm{d}\Omega$. The appearance in Eq. (14.52) of this angular dependence is not through the function $\zeta(\theta,\phi)$, since here we consider the power flow through a plane, whereas $\mathrm{d}P/\mathrm{d}\Omega$ refers to the power flow through a sphere. The third line in Eq. (14.52) originates in the possible rotation of the field lines near the source. This is most easily seen from the fact that this term changes sign with the sign of β. The overall factor of $1/(q_{\rm o}q)$ indicates that this term vanishes rapidly in the far field, as compared to the remaining terms in braces. We shall see below, however, that a finite and observable effect of this term survives in the far field.

14.9. Linear Dipole

Let us first consider $\beta = 0$, corresponding to a linear dipole, oscillating along the *y*-axis. The intensity distribution (52) on an image plane then becomes

$$I(\mathbf{r}_{\rm o};\lambda,\mu) = I_{\rm o}\left(\frac{q_{\rm o}}{q}\right)^3 \left[1 - \frac{1}{q^2}(\overline{\rho}\sin\phi_{\rm o} + \overline{\mu}\cos\phi_{\rm o})^2\right] . \tag{14.55}$$

For a linear dipole, all field lines are straight, and any dependence of the intensity on $\mathbf{r}_{\rm o}$, λ and μ comes from the angular dependence of $\mathrm{d}P/\mathrm{d}\Omega$ and from the fact that we cut through $\mathrm{d}P/\mathrm{d}\Omega$ with a plane. As an illustration, let us consider an observation plane perpendicular to the *y*-axis at the positive side. We then have $\theta_{\rm o} = \pi/2$, so $\overline{\rho} = q_{\rm o}$, and $\phi_{\rm o} = \pi/2$. We introduce angle γ as the observation direction for a point

in the image plane, as seen from the site of the dipole (see Fig. 14.6). We then have $\cos\gamma = q_{\mathrm{o}} / q$, and the intensity becomes

$$I(\mathbf{r}_{\mathrm{o}};\lambda,\mu) = I_{\mathrm{o}} \cos^3\gamma \sin^2\gamma \ . \tag{14.56}$$

Since the right-hand side of Eq. (14.56) only depends on angle γ, the intensity distribution in the image plane is circularly symmetric around the origin. At the origin of the image plane we have $\gamma = 0$ and therefore $I = 0$, which corresponds to the well-known fact that no radiation is emitted along the dipole axis for a linear dipole. The intensity has a maximum for $\cos\gamma = \sqrt{3/5}$, corresponding to an angle of $\gamma = 39^{\mathrm{o}}$, and this defines a ring in the observation plane. The radius of this ring is $q_{\mathrm{o}}\sqrt{2/3}$. The intensity profile is shown in Fig. 14.8.

14.10. Rotating Dipole and the Far Field

The intensity distribution in Fig. 14.8 scales with the distance q_{o} between the dipole and the observation plane, which is a reflection of the fact that the field lines of the Poynting vector are straight for a linear dipole. When the image plane moves further away, the picture remains the same, apart from a scale factor. We now consider the effect of the rotation of the field lines near the source for a rotating dipole moment on the intensity profile in the far field. We first look at a circular dipole for which $\beta = \pm 1$. The intensity on the image plane, given by Eq. (14.52), simplifies for $\beta = \pm 1$ to

$$I(\mathbf{r}_{\mathrm{o}};\lambda,\mu) = I_{\mathrm{o}}\left(\frac{q_{\mathrm{o}}}{q}\right)^3 \left[1 - \frac{1}{2q^2}(\overline{\rho}^2 + \overline{\mu}^2)\right.$$

$$\left. - \frac{\beta}{q_{\mathrm{o}} q}\left(1 + \frac{1}{q^2}\right)\overline{\mu}\sin\theta_{\mathrm{o}}\right] . \tag{14.57}$$

There is no dependence on the observation angle ϕ_{o}, as could be expected for a circular dipole moment in the *xy*-plane.

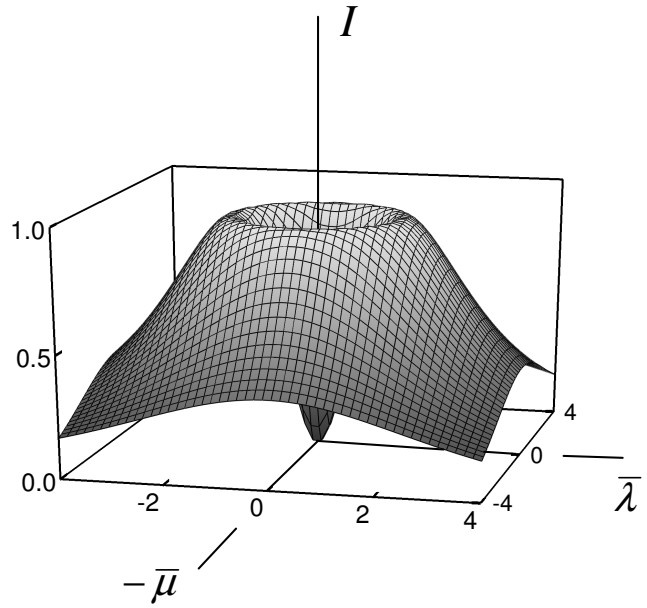

Fig. 14.8. The figure shows the intensity distribution on an image plane for a linear dipole. The plane is perpendicular to the dipole axis.

We are looking for effects in the far field that are due to the rotation of the field lines near the source. The displacement from Sec. 14.7 was maximum for observation in the *xy*-plane, e.g. $\theta_{\rm o} = \pi/2$, so here we consider the same situation in order to find the maximum effect. From Eq. (14.53) we then have $\overline{\rho} = q_{\rm o}$, and from Eq. (14.57) we see that the dependence on the coordinate λ in the image plane only enters through the λ dependence of q in Eq. (14.51). Therefore, the intensity only depends on λ as λ^2, and consequently there is an extremum at $\lambda = 0$. With $\theta_{\rm o} = \pi/2$ and $\lambda = 0$, Eq. (14.57) becomes

$$I(\mathbf{r}_{\rm o};0,\mu) = I_{\rm o}\left(\frac{q_{\rm o}}{q}\right)^3\left[\frac{1}{2} - \frac{\beta}{q_{\rm o}q}\left(1+\frac{1}{q^2}\right)\overline{\mu}\right], \qquad (14.58)$$

which is the intensity along the μ axis in the image plane. To find the extrema, we set $\partial I/\partial\overline{\mu} = 0$. This yields

$$\frac{3}{2}\overline{\mu} = -\frac{\beta}{q_{\mathrm{o}} q}\left[1 + q_{\mathrm{o}}^2 - 3\overline{\mu}^2\left(1 + \frac{2}{q^2}\right)\right] . \tag{14.59}$$

In the far field we have $q_{\mathrm{o}} >> 1$, and Eq. (14.59) becomes

$$\frac{3}{2}\overline{\mu} = -\frac{\beta}{q_{\mathrm{o}} q}(q_{\mathrm{o}}^2 - 3\overline{\mu}^2) . \tag{14.60}$$

We are looking for a possible shift in the intensity profile due to the rotation of the field lines. Such a shift has to remain finite for $q_{\mathrm{o}} \to \infty$, as can be seen from Fig. 14.7, so at such an extremum we must have $\overline{\mu} / q_{\mathrm{o}} \to 0$ for q_{o} large. If we indicate by $\overline{\mu}_{\mathrm{p}}$ the solution of Eq. (14.60), we find for the location of the peak in the intensity profile

$$\overline{\mu}_{\mathrm{p}} = -\frac{2}{3}\beta . \tag{14.61}$$

The magnitude of this shift is 2/3 in dimensionless coordinates, and since 2π corresponds to one wavelength, the shift is equal to a wavelength divided by 3π. Apparently, this is a nanoscale shift for optical radiation, but it is a shift that persists in the far field. Figure 14.9 shows the intensity distribution for this case.

For Fig. 14.9 we took $q_{\mathrm{o}} = 4$ (and $I_{\mathrm{o}} = 1$), which is $2/\pi$ times a wavelength. This is just enough to justify the far-field approximation $q_{\mathrm{o}} >> 1$. For larger values of q_{o}, the background becomes very large since it scales with q_{o}, and it may not be possible experimentally to resolve the shift of the peak. In an experiment, the dipole is set in oscillation with a laser beam. A circular dipole moment in the *xy*-plane is induced by a circularly polarized laser beam, propagating along the *z*-axis, and the sign of β is determined by the helicity of the laser. In Eq. (14.57), the first line is the broad background and the second line is due to the rotation of the field lines. The background does not depend on the sign of β, so if we would measure the intensity for left- and right-handed helicity then the difference of the profiles would be twice the second line of Eq. (14.57), and any resulting difference profile would be due entirely to the rotation of the field lines. This experiment was performed recently [7] and such an asymmetric profile was found indeed.

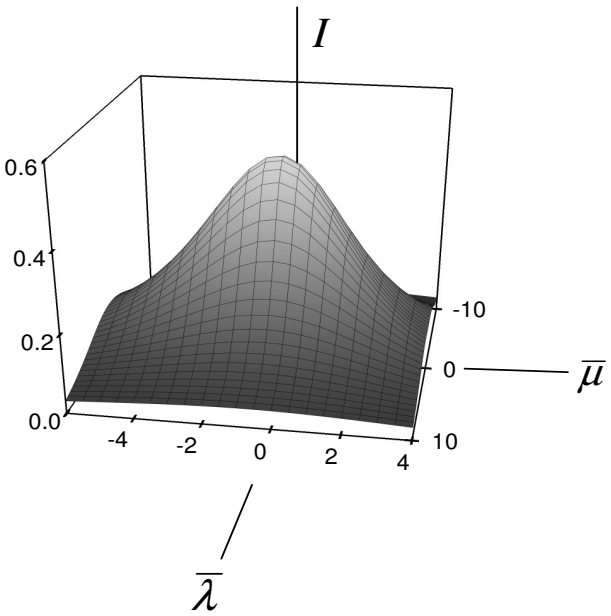

Fig. 14.9. The figure illustrates the nanoscale shift of the intensity profile for a circular dipole. The image plane is the same as in Fig. 14.8.

For an elliptical dipole, similar calculations show [6] that the profile is more complicated. It can have maxima, minima and saddle points. In particular, the maximum shown in Fig. 14.9 can become a minimum, and the effect of the rotation of the field lines can be a moving hole rather than a moving peak.

14.11. Intensity in the Near Field

With very precise near field techniques, involving fiber tip probes, intensities can be measured in the near field with nanoscopic precision [8,9]. In this approach the existence of the vortex could be verified experimentally by measuring the intensity directly at the location of the vortex, rather than through the observation of the displacement of the maximum of the intensity profile in the far field. Figure 14.10 shows the intensity distribution on an image plane very close to a circular dipole, for the case where the image plane is perpendicular to the y-axis. Near

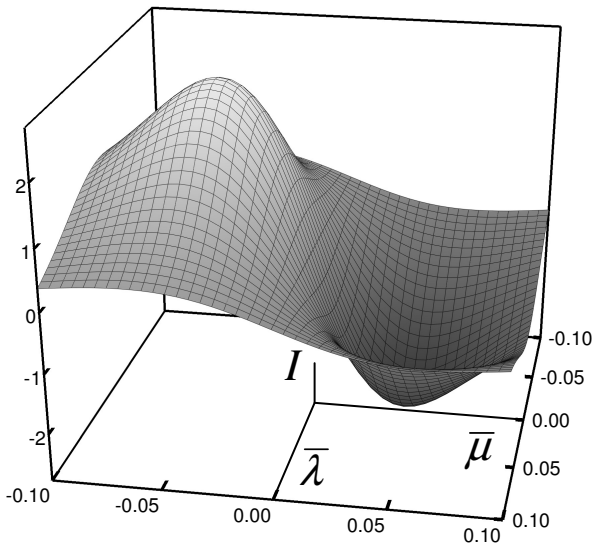

Fig. 14.10. The figure shows an intensity profile in the near field of a circular dipole.

the positive peak, the field lines pass through the image plane in the outward direction. The negative peak indicates that in this region of the observation plane the field lines are inward. This image is a direct consequence of the spiraling of the field lines near the source. A field line first passes through the image plane in the outward direction, and then spirals back inwards near the peak with negative intensity. Although it may not be possible to measure a negative intensity directly in an experiment, the figure nevertheless illustrates the winding of the field lines in an appealing manner.

14.12. Conclusions

When an electric dipole moment rotates in the *xy*-plane, the field lines of energy flow swirl numerous times around the *z*-axis, while remaining on the surface of a cone. Far away from the dipole, the field lines approach asymptotically a straight line, reminiscent of an optical ray. This line is displaced with respect to the radial direction, and this leads to an apparent shift of the dipole location, when viewed from far away. This

displacement depends on the observation direction and on the eccentricity of the ellipse. In order to define an image of the dipole, we have considered the intensity distribution of the emitted radiation over an image plane. For a circular dipole, the image is a single peak when viewed in the plane of rotation of the dipole. It was shown that in the far field the peak of this intensity profile is shifted with respect to the central direction, and that this shift is due to the rotation of the field lines near the source. In this fashion, the near field curving of the field lines affects the image in the far field, and this makes the vortex near the dipole observable at a macroscopic distance. The shift is of the order of a fraction of a wavelength, as is the dimension of the vortex.

References

1. M. Born and E. Wolf, *Principles of Optics*, 6th edn. (Pergamon, 1980), Chapter 3.
2. J. D. Jackson, *Classical Electrodynamics*, 3rd edn. (Wiley, 1991), p. 411.
3. I. V. Lindell, *Methods for Electromagnetic Field Analysis* (Oxford U. Press, 1992), Section 1.4.
4. L. Mandel and E. Wolf, *Optical Coherence and Quantum Optics* (Cambridge U. Press, 1995), p. 469.
5. J. Shu, X. Li and H. F. Arnoldus, Energy flow lines for the radiation emitted by a dipole, *J. Mod. Opt.* **55**, 2457–2471 (2008).
6. J. Shu, X. Li and H. F. Arnoldus, Nanoscale shift of the intensity distribution of dipole radiation, *J. Opt. Soc. Am. A* **26**, 395–402 (2009).
7. D. Haefner, S. Sukhov and A. Dogariu, Spin Hall effect of light in spherical geometry, *Phys. Rev. Lett.* **102**, 123903 1–4 (2009).
8. K. G. Lee, H. W. Kihm, J. E. Kihm, W. J. Choi, H. Kim, C. Ropers, D. J. Park, Y. C. Yoon, S. B. Choi, D. H. Woo, J. Kim, B. Lee, Q. H. Park, C. Lienau and D. S. Kim, Vector field microscopic imaging of light, *Nat. Photonics* **1**, 53–56 (2007).
9. Y. Ohdaira, T. Inoue, H. Hori and K. Kitahara, Local circular polarization observed in surface vortices of optical near-fields, *Opt. Exp.* **16**, 2915–2921 (2008).